1974-02

Experimental verification of density inhomogeneity due to lasing in a gas-dynamic laser

Fuhs, A.E.

Experimental verification of density inhomogeneity due to lasing in a gas-dynamic laser

A. E. Fuhs and O. Biblarz

Naval Postgraduate School, Monterey, California 93940

J. K. Cawthra

Laser Division, Air Force Weapons Laboratory, Albuquerque, New Mexico 87100

J. L. Campbell

Pratt and Whitney Aircraft, Florida Research and Development Center, West Palm Beach, Florida 33401
(Received 1 October 1973; in final form 15 November 1973)

As a consequence of lasing, heat, in an amount related to the quantum efficiency, is released in a gas-dynamic laser (GDL) causing density perturbations, Calculations were made to predict the density contours throughout the laser cavity. Subsequent to the calculations, density changes due to lasing were measured using a Mach-Zehnder interferometer. The predicted and observed density variations were in good agreement.

Knowledge about beam quality plays an important role in the design of near-diffraction-limited gas-dynamic lasers (GDLs). Of all the things that influence beam quality, changes in density due to heat release have until recently[1,2] been neglected. Some heat release is inherent in a three-level molecular laser, and this heat is accounted for in the laser quantum efficiency. For the CO_2 laser operating at 10.6 μ, at least 60% of the upper laser energy appears as heat in the gas.

The perturbations due to heat addition in a supersonic free stream are well understood. Heating generates compression waves which radiate along the characteristics and reflect from the cavity walls. Downstream of the heat release region is a wake which, unlike the compression waves, decreases the gas density.

Density gradients due to heat release cause phase changes within the laser cavity similar to those gradients caused by thermal blooming. Typical laser beam intensity distributions are not homogeneous and the heating effect is more complicated than the classical one-dimensional or Rayleigh flow problem. Estimates[2] of density changes within the beam due to the depopulation of the lower laser level indicate that density changes can be in the order of 1 or 2% for CO_2. A computer code designed to account for a two-dimensional interaction, including wall reflections and kinetics of energy release, predicts density changes of over 12% for an unstable oscillator output in a region located three beam diameters downstream of the beam. This prediction was verified experimentally in the facility described in this letter. It is clear that a laser system which proposes to have multiple beam passes will be adversely

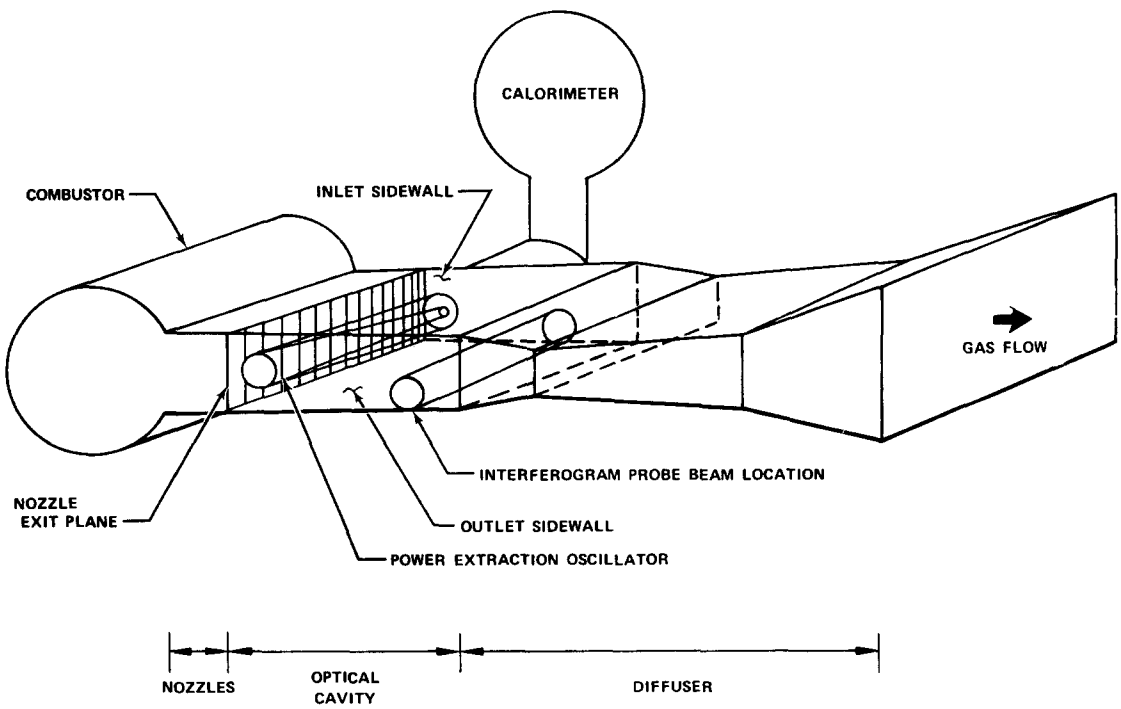

FIG. 1. Schematic of GDL used in tests.

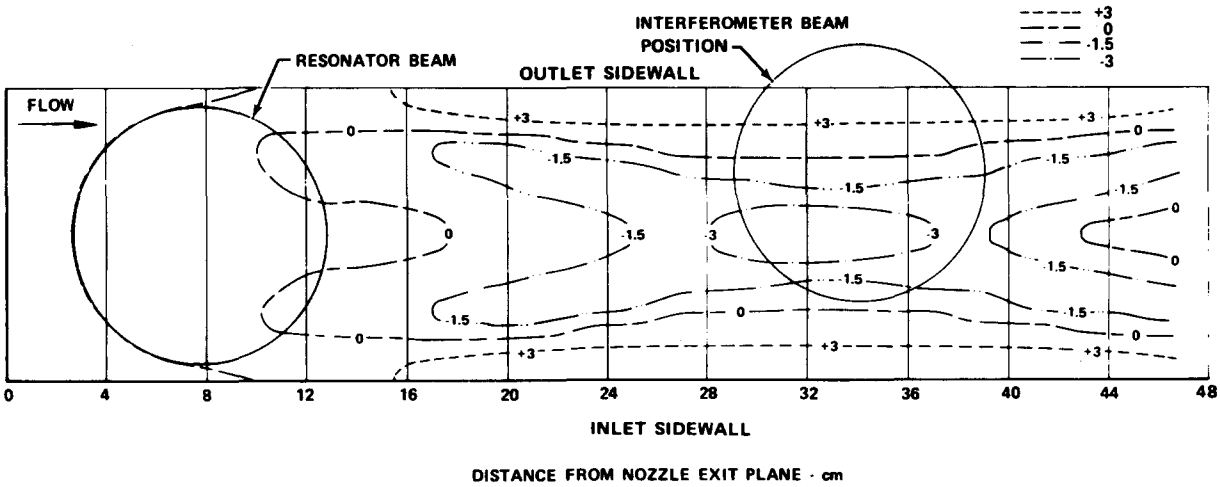

FIG. 2. Isodensity contour plot of predicted density field, $\Delta\rho/\rho$, in percent.

affected by this "optically dirty" gas downstream of the first pass. The CO-pumped CO_2 laser represents one such example.

The model used for the description of the density perturbations assumes that the flow is two-dimensional, planar, nonviscous, and nonheat-conducting. Variations along the laser beam are less significant due to averaging. Tsien and Beilock[3] obtained solutions for the linearized equations of motion with heat addition from line sources. Fuhs[1] modified the equations to obtain an integral representation, which in terms of a fractional density perturbation $\Delta\rho/\rho$ becomes

$$\frac{\Delta\rho(x,y)}{\rho}=\frac{(\gamma-1)M}{2a^3\beta\rho}\int_0^S h(x,y')\sin\mu\,dS \qquad (1)$$
$$-\frac{(\gamma-1)}{a^2\rho U}\int_{x'}\int_{y'} h(x',y')\delta(y'-y')I(x'-x')\,dx'\,dy'.$$

The symbols in Eq. (1) have the following meaning: γ is the heat capacity ratio; M is the Mach number and a is the speed of sound; $\beta=(M^2-1)^{1/2}$; U is the gas velocity; S is the distance along a characteristic and μ is the Mach angle; $h(x',y')$ is the heat release per unit volume per unit time; I is the impulse function and δ is the Dirac delta function. The first integral in Eq. (1) gives the contribution from the compression waves and the second provides the expansion in the wake.

The heat release function at a point x' corresponding to lasing at ξ, $h(x',y')$, is related to the power density at the laser aperture, $i(\xi,y')$, by

$$h(x',y')=C\int_{x_u}^{x'} i(\xi,y')\exp[-(x'-\xi)/U\tau]\,d\xi, \qquad (2)$$

where x_u is the upstream beam boundary and C is a constant that is evaluated by an energy balance. The exponential term in the integrand accounts for the fact that the heat release is controlled by a vibrational-translational relaxation. The relaxation time is τ. $h(x',y')$ has the shape of a Gaussian when the laser cavity serves as an amplifier and of a crescent when the GDL is run as an unstable oscillator (UO). For a more detailed discussion of Eqs. (1) and (2), see Biblarz and Fuhs.[2]

Equation (2) assumes that the only heat release is that due to the collisional depopulation of the lower laser level. Relaxation from other vibrational levels contribute to $h(x',y')$. A simplified kinetics model involving these energy levels has been formulated and results indicate that the dominant factor is the energy due to the relaxation of the lower laser level.

Equation (1) was programmed for the calculation of a two-dimensional field where the energy release distribution is known. Results from this program were checked against calculations from the AFWL HYDRO code[4] which solves the nonlinearized set of equations, and the comparison was quite excellent.

The computer program was run using as input data the nominal run conditions of an operational well-characterized GDL. On the basis of these predictions a test series was designed to detect the presence of density inhomogeneities induced by power extraction. The measurement technique was Mach-Zehnder inteferometry and shadowgraph flow visualization in a selected area

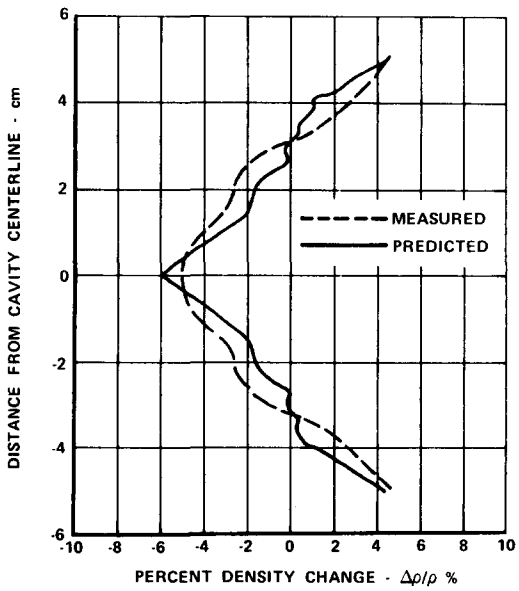

FIG. 3. Comparison of measured and predicted density field at the interferogram observation location.

TABLE I. Loaded interferometry test conditions.

Cavity static temperature (°K)	310
Cavity static pressure (atm)	0.044
Composition (%)	
N_2	79.5
CO_2	15.0
H_2	1.1
CO	2.7
O_2	1.7
Interferometer sensitivity, $\frac{\%\Delta\rho/\rho}{\text{fringe shift}}$	2.8

in the cavity. The apparatus schematic is shown in Fig. 1. Measurements were done without power extraction and then repeated with power extraction. The laser was operated as an UO with a geometric coupling of 0.80. The entire output beam was directed into a calorimeter for the determination of the power in the beam.

The location of the interferometric equipment was coincident with the predicted region of maximum density perturbation. The probe beam position was offset from the centerline toward the side known to have the weakest aerodynamic disturbances. These arise from viscous phenomena in the nozzles, wall displacements due to heating, etc.

Nominal operating conditions for the experiment are shown in Table I. The interferograms were recorded by high-speed movie cameras. Frames recorded at equivalent times from the start signal were compared for both no power and power extraction. It was assumed that the density changes due to heat addition could be superimposed on the density pattern due to aerodynamic disturbances. Under these assumptions, which are consistent with the linearized equations solution, the differences between the interferograms of the two cases could be interpreted as the density perturbations resulting from power extraction.

The computer program was then rerun using the reported operating conditions, and the isodensity contours shown in Fig. 2 were obtained. For τ in Eq. (2), a value of 8 μsec was used. The measured and predicted density variations are plotted as a function of the distance from the cavity centerline in Fig. 3. As can be seen, both the trend of the density variation and the magnitude of the change are accurately predicted by the theory.

On the basis of the information presented here, the model for the calculation of density inhomogeneities due to heat release appears to be adequate. The kinetics model used is not very sophisticated and perhaps refinements will provide for better agreement in the regions near the wall.

[1]A.E. Fuhs, AIAA J. 11, 374 (1973).
[2]O. Biblarz and A.E. Fuhs, AIAA Paper No. 73-414, 1973 [AIAA J. (to be published)].
[3]H.S. Tsien and M. Beilock, J. Aeronaut. Sci. 16, 756 (1949).
[4]D.B. Mitchell, J.K. Cawthra, and M.L. Havens, Laser Digest No. AFWL TR73-131, pp. 300—308, 1973 (unpublished).

Real-time synchronously pulsed ir image up-conversion

D. Y. Tseng

Hughes Research Laboratories, Malibu, California 90265
(Received 5 November 1973)

Real-time ir image up-conversion has been achieved using a synchronously pulsed mode of operation for both the pump and ir sources. Operating at 133 pulses/sec, the up-converted images were readily viewed on an ordinary S-1 surface image intensifier tube. Optimization and adjustments of image quality were accomplished easily in real time.

A new mode of operation for ir up-conversion was reported recently in which both the ir and pump sources were operated in a pulsed mode.[1] Up-conversion was obtained by synchronizing these pulses to achieve nonlinear mixing in an appropriate crystal. Under these conditions both high-efficiency operation and high-power output at the up-converted wavelength were achieved simultaneously. Specifically, a peak power of 8.4 W at the up-converted wavelength and power conversion efficiency of 0.84% were obtained previously in up-converting 10.6-μm radiation to 0.96-μm. Subsequently, by increasing the pump power these figures have been further improved to 20-W peak output power and 2% power conversion efficiency. This scheme of operation is directly applicable to active (pulse-illuminated) ir image up-conversion systems.

This paper reports the utilization of the synchronously pulsed mode of operation for use in ir image up-conversion. Because of the above-mentioned basic advantages of this scheme, real-time up-converted images were easily obtained and readily observed on an ordinary S-1 surface image intensifier tube (RCA 6914A). The image up-converter was operated at 133 pulses/sec (pps). Based on the published literature, this represents the first demonstration of real-time 10-μm image up-conversion. Previous 10-μm image up-conversion results have been viewed either on a single-